Direct Generation of Tailored Pulse-Mode Entanglement

Francesco Graffitti [ORCID],[1,*,†] Peter Barrow,[1,†] Alexander Pickston,[1] Agata M. Brańczyk [ORCID],[2] and Alessandro Fedrizzi [ORCID][1]

[1]*Institute of Photonics and Quantum Sciences, School of Engineering and Physical Sciences, Heriot-Watt University, Edinburgh EH14 4AS, United Kingdom*
[2]*Perimeter Institute for Theoretical Physics, Waterloo, Ontario N2L 2Y5, Canada*

Photonic quantum technology increasingly uses frequency encoding to enable higher quantum information density and noise resilience. Pulsed time-frequency modes (TFM) represent a unique class of spectrally encoded quantum states of light that enable a complete framework for quantum information processing. Here, we demonstrate a technique for direct generation of entangled TFM-encoded states in single-pass, tailored down-conversion processes. We achieve unprecedented quality in state generation— high rates, heralding efficiency, and state fidelity—as characterized via highly resolved time-of-flight fiber spectroscopy and two-photon interference. We employ this technique in a four-photon entanglement swapping scheme as a primitive for TFM-encoded quantum protocols.

Generating entanglement in intrinsically high-dimensional degrees of freedom of light, such as transverse and longitudinal spatial modes [1,2], or time and frequency, constitutes a powerful resource for photonic quantum technologies— photons that carry more information enable more efficient protocols [3,4]. Time-frequency encoding is intrinsically suitable for waveguide integration and fiber transmission [5,6], making it a promising choice for practical, high-dimensional quantum applications. Quantum information can be encoded either in discrete temporal or spectral modes (namely time- and frequency-bin encoding [6–9]) or in the spectral envelope of the single-photon wave packets—time-frequency mode (TFM) encoding [5,10]. TFM-encoded states arise naturally in parametric down-conversion (PDC) sources, as TFMs are eigenstates of the PDC process and they span an infinite-dimensional Hilbert space. Conveniently, TFMs possess highly desirable properties: being centered around a target wavelength makes them compatible with fiber networks, they are robust against noise [11] and chromatic dispersion [12], their pulsed nature enables synchronization and therefore multiphoton protocols and they offer intrinsically high dimensionality [10]. Manipulation and detection of TFMs is enabled by the quantum-pulse toolbox, where sum-and difference-frequency generation are used for reshaping and projecting the quantum states [5,10]. However, generating entangled TFMs in a controlled way can be very challenging [13–17], limiting their usefulness in realistic scenarios. Here, we overcome this problem exploiting domain-engineered nonlinear crystals [18,19] for generating TFM entanglement from standard ultrafast laser pulses in a single-pass PDC experiment. We experimentally validate this technique by benchmarking a maximally antisymmetric state at telecom wavelength with near unity fidelity, and implement a four-photon entanglement swapping scheme. Our work complements the pulse-gate toolbox [5,10] for TFM quantum information processing, and establishes a standard for the generation of TFM quantum states of light while paving the way for more complex frequency encoding.

In a PDC process, a pump photon probabilistically down-converts into two photons under momentum and energy conservation. The second-order nonlinearity of a crystal mediates the process through the phase-matching function (PMF) which, together with the pump spectral profile, dictates the spectral properties of the output biphoton state in the form of its joint spectral amplitude (JSA). The spectral entanglement between the PDC photons is quantified by the Schmidt number via Schmidt decomposition of the JSA [20]: a separable, unentangled JSA has a Schmidt number of 1; higher values indicate the presence of entanglement. Conveniently, this decomposition also provides the spectral modal structure of the PDC biphoton state. TFMs can therefore be engineered by shaping the JSA, either by modifying the pump-pulse amplitude function [10] or, as we demonstrate here, by shaping the PMF via nonlinearity engineering. Domain-engineered crystals have been employed successfully for the generation of spectrally pure heralded photons [18,19], where undesired frequency correlations are eliminated by tailoring a Gaussian nonlinearity profile. Here we extend this technique to the direct, controlled generation of custom TFM entanglement.

We use the Hermite-Gauss modes [10] basis to encode the TFM quantum state, with the goal of generating the maximally entangled antisymmetric Bell state:

$$|\psi^-\rangle_{s,i} = \frac{1}{\sqrt{2}} \left(|\wedge\rangle_s |\vee\vee\rangle_i - |\vee\vee\rangle_s |\wedge\rangle_i \right), \quad (1)$$
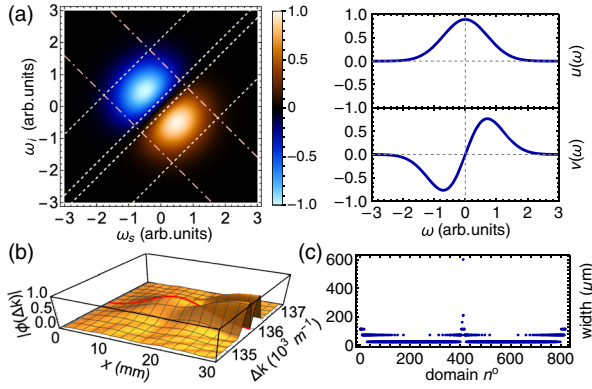
FIG. 1. Crystal engineering. (a) Maximally entangled JSA (left) and corresponding TFM basis states, $u(\omega)$, $v(\omega)$ (right). The pink dot-dashed lines and the yellow dashed lines are the $1/e$ contours of the pump's and PMF's amplitudes, respectively. (b) Target phase-matching function along the crystal at different momentum mismatch (ΔK) values: the tracking algorithm chooses the domain orientation to track the PMF at the quasi-phase-matching condition $\Delta K = \Delta K_0$, as shown by the red trace. (c) Target crystal domain structure.

where "s" ("i") labels the signal (idler) photon. The state (1) corresponds to the joint spectrum encoded in the TFM basis states $\wedge = u(\omega)$ and $\vee = v(\omega)$ in Fig. 1(a) (see the Supplemental Material [21], Sec. 1 for details on the biphoton spectral structure). We use our recently developed nonlinearity-engineering algorithm [18] to shape the PMF $[\phi(x, \Delta k)]$ as a first-order Hermite-Gauss function. We design a 30 mm potassium titanyl phosphate (KTP) crystal for symmetric group-velocity matching with a 1.3 ps laser pulse [20]. The fundamental domain width is ~ 23.1 μm, equal to the coherence length of a 775 nm pump down-converted into two 1550 nm photons. Our algorithm chooses the ferroelectric orientation of individual domains to track a target PMF along the field propagation in the crystal (see the Supplemental Material [21], Sec. 2 for details on the algorithm). Figures 1(b) and 1(c) show the resulting PMF $[\phi(\Delta k)$ at $x = 30$ mm] and the required crystal domain configuration.

The designed crystal was manufactured commercially by *Raicol Ltd.* We set up a collinear PDC source [19], where a 80 MHz, pulsed Ti:sapphire laser is focused into the tailored KTP crystal to create orthogonally polarized photon pairs via type-II PDC. The photons are loosely filtered with a bandpass filter (~ 3 times broader than the PDC photons' bandwidth). A polarizing beam splitter separates the PDC photons before they are coupled into single-mode fibers. We measured a source brightness of ~ 4 KHz/mW photon pairs with a symmetric heralding efficiency $> 60\%$, a reasonable trade-off achieved by optimizing the pump, signal, and idler focusing conditions [19].

A full characterization of the biphoton quantum state could be obtained via quantum state tomography in the TFM basis, which requires projective measurements onto

three mutually unbiased bases using cascades of tailored nonlinear processes [22–24], or by reconstructing the JSA including its phase, which assumes a pure biphoton state and involves complex interferometric techniques [25–27]. We instead characterize the PDC state using an indirect approach that exploits joint spectral intensity (JSI) reconstruction via dispersive fiber spectroscopy [28] and two-photon interference [Hong-Ou-Mandel (HOM) effect [29]] to infer information on the populations and the entanglement of the quantum state, respectively.

The setup for the JSI reconstruction is shown in Fig. 2(a) (modes I). Each photon is sent through a ~ 20 km single-mode fiber to convert spectral to temporal information exploiting the fiber dispersion of ~ 18 ps/km/nm at 1550 nm. The photons are then detected with superconductive nanowire single photon detectors (SNSPD), with $\sim 80\%$ detection efficiency and < 50 ps timing jitter. Arrival times are recorded as time tags by a *Picoquant HydraHarp* in 1 ps bins for offline processing. We collected $\sim 2.8 \times 10^6$ two-photon coincidence counts with respect to a clock signal, used to center the JSI plots, in 24 hours. The clock consisted of a third SNSPD triggered by an independent PDC source pumped by the same laser (more details provided in the Supplemental Material [21], Sec. 3). We reconstruct the JSI over a 36 nm spectral range, ~ 12 times larger than the PDC photons' bandwidth, to ensure reliable estimation of the JSI properties [20]. The results are shown in Fig. 3(a). The overlay contours show the theoretical pump spectrum and the expected PMF (assuming the ideal crystal domain structure and a sech^2 pump function). There is excellent correspondence between the
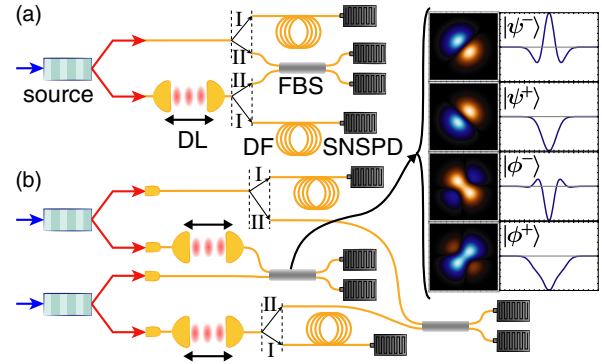

FIG. 2. Experimental setup. (a) Biphoton state characterization: joint-spectrum reconstruction via dispersive fiber (DF) time-of-flight spectroscopy (modes I) and HOM interference in a fiber beam splitter (FBS) (modes II). (b) Entanglement swapping setup: successful entanglement swapping is heralded by a coincidence detection of the photons after the FBS. The swapped state is again verified via fiber spectroscopy (modes I) and HOM interference (modes II). We note that a setup similar to (modes I) has been used to investigate the spectral properties of HOM interference [30]. The panel on the right shows the four possible Bell-state projections at the BS, and the corresponding interference pattern.
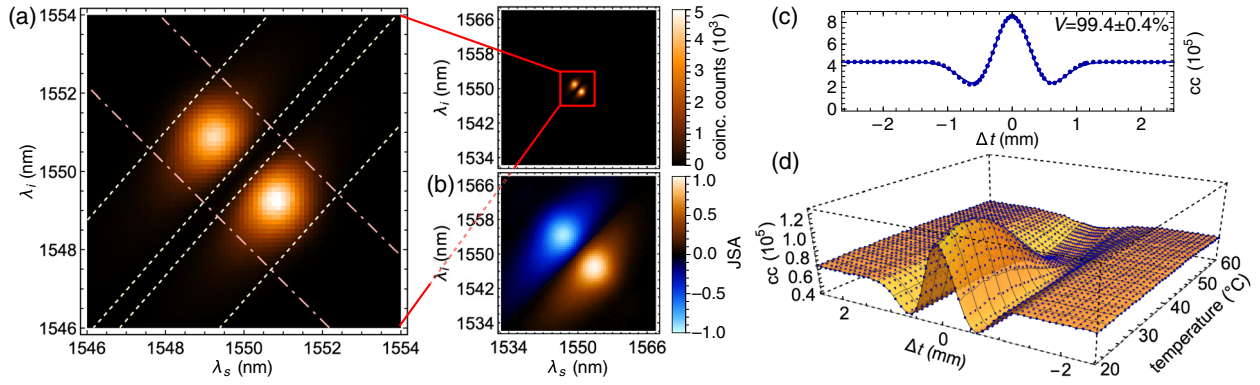
FIG. 3. Single source characterization. (a) Measured JSI (right) and zoom on a reduced, 8 nm spectral range (left) to show its main features. The bin size corresponds to 0.118 nm (see the Supplemental Material [21], Sec. 6 for details). The dot-dashed pink lines and yellow dashed lines are the $1/e^2$ contours of the sech^2 pump's intensity, and of the PMF's absolute value squared calculated from the crystal domain structure, respectively. (b) Reconstructed effective JSA. (c) Signal-idler interference pattern. (d) Signal-idler interference varying crystal temperature. The HOM visibility has a maximum at 25 degrees, while no antibunching occurs above 39 degrees. Error bars assuming Poissonian counting statistics are smaller than the symbol size.

theoretical target and the measured JSI, which faithfully reproduces not only the two main peaks but also the spectral bandwidth.

The HOM setup is shown in Fig. 2(a), modes II: the interference pattern is measured by delaying one photon with respect to the other before they interfere in a fiber BS. While two-photon interference is typically destructive and, for PDC photons, exhibits a characteristic triangular or Gaussian "dip" [19], antibunching at the BS can occur whenever the biphoton state is at least partially antisymmetric under particle exchange: more antisymmetry results in more antibunching [31] (see the Supplemental Material [21], Sec. 4 for proof). Remarkably, for a biphoton state that is separable in all other DOFs, antibunching corresponds to entanglement in the biphoton spectrum [32]. We use this result to verify TFM entanglement in our generated state. We show the experimental data in Fig. 3(c): the fitted HOM visibility is equal to $99.4 \pm 0.4\%$, certifying a high degree of spectral entanglement of the PDC biphoton state (the fitting function is given in the Supplemental Material [21], Sec. 1).

Finally, HOM interference between heralded PDC-photons generated by two identical sources can be used to estimate the Schmidt number of the biphoton state [19,33]: since the $|\psi^-\rangle$ state in Eq. (1) is composed of two equally weighted TFM basis states, the corresponding Schmidt number is expected to be equal to 2. We measure a HOM visibility of $48.8 \pm 1.2\%$ at 30 mW of average pump power (see the Supplemental Material [21], Sec. 5 for details), which corresponds to a Schmidt number of 2.05 ± 0.05, in excellent agreement with theory.

While the JSI reconstruction doesn't contain any phase information, we can exploit our knowledge of the antisymmetry and Schmidt number of the biphoton wave function to reconstruct an "effective" JSA. Specifically,

to guarantee antisymmetry and bimodal structure of the quantum state, we impose an $e^{i\pi}$ sign shift between the two peaks of the square root of the measured JSI. This antisymmetric phase shift matches, up to an additional linear phase, the output of the nonlinearity-engineering algorithm that generates the state in Eq. (1). The true JSA might instead have nonlinear phase terms, as long as they do not affect the Schmidt number we obtained from the heralded-photon HOM measurement (see the Supplemental Material [21], Sec. 5 for further discussion). The effective JSA obtained in this way is depicted in Fig. 3(b). It qualitatively matches the theoretical target JSA shown in Fig. 1(a) and has an effective Schmidt number of 2.026 ± 0.001, consistent with the HOM measurement and with our numerical simulations (details on the JSI reconstruction and error estimation are discussed in the Supplemental Material [21], Sec. 6).

Small variations in the crystal domain widths can be introduced by changing the crystals temperature. This results in a shift of the PMF in the (ω_s, ω_i) plane, producing frequency nondegenerate photons and therefore compromising the antisymmetry of the biphoton wave function. Surprisingly, this doesn't affect the Schmidt number of the quantum state: the biphoton state (1) remains intact, but the signal and idler TFMs are centered around different frequencies. This enables the capability of switching between an antisymmetric state to a nonantisymmetric one without spoiling the spectral modal structure. We observe the biphoton antisymmetry breaking by performing HOM scans at different temperatures, from 20 to 60 degrees at 1 degree intervals. We show the results in Fig. 3(d): antibunching (and therefore antisymmetry) is maximal for perfectly degenerate PDC and it reduces as we tune away from degeneracy, until no antibunching occurs above a certain center-frequency offset, as expected from theory.

Multiphoton protocols using TFMs will require the ability to interfere and swap independently generated TFM-encoded photons. While a generalized entanglement swapping for TFM has been proposed, it relies on a nonlinear process between two single photons and therefore has very low success probability [34]. Here we instead implement the standard entanglement swapping scheme with the setup shown in Fig. 2(b). Two entangled $|\psi^-\rangle$ states are produced via two independent engineered TFM-entangled pair sources. The overall four-photon state can be written as $1/2(|\phi^+\rangle|\phi^+\rangle + |\phi^-\rangle|\phi^-\rangle + |\psi^+\rangle|\psi^+\rangle - |\psi^-\rangle|\psi^-\rangle)$, a coherent sum of the four Bell states:

$$\begin{aligned} |\psi^\pm\rangle &= \frac{1}{\sqrt{2}} |\curlywedge\rangle |\curlyvee\rangle \pm |\curlyvee\rangle |\curlywedge\rangle \\ |\phi^\pm\rangle &= |\curlywedge\rangle |\curlywedge\rangle \pm |\curlyvee\rangle |\curlyvee\rangle. \end{aligned} \tag{2}$$

The joint spectra for all four Bell states and the corresponding HOM patterns are shown in the inset of Fig. 2(b): perfect antibunching at the BS occurs only for the singlet state, while triplet states bunch due to the symmetry of their wave functions. We use this to discern a successful projection on $|\psi^-\rangle$ from all the other outcomes: a two-photon coincidence detection at the two BS outputs corresponds to a projection on the singlet state and heralds swapping of the TFM $|\psi^-\rangle$ state from the two original photon pairs to the two non-interacting photons (see the Supplemental Material [21], Sec. 3 for details).

We benchmark the state obtained after entanglement swapping via fiber spectroscopy and HOM interference, as shown in Fig. 2(b), modes I and II, respectively. The JSI of the swapped $|\psi^-\rangle$ state is again measured by sending the two photons through a pair of 20 km fibers. In Fig. 4(a) we show the measured joint spectrum of the two-photon state without postselection heralded by either one or two detection events after the BS, corresponding to threefold and fourfold coincidence counts, respectively. We collect 670k threefold and ~46k fourfold coincident counts in 72 hours of integration time. We observe four peaks, arising from a mixture of the four equally weighted Bell state JSAs [see Fig. 2(b)]. When we instead record fourfold coincident counts, we measure the spectrum of the swapped $|\psi^-\rangle$ biphoton state, recovering the two main peaks on the JSI's diagonal [Fig. 4(b)].

We then measure the HOM interference of the swapped state. Because the probability of generating photon pairs independently equals that of a double-pair emission in each source, the maximal theoretical HOM visibility is 25%—not a fundamental limitation, it only occurs when both photons of two PDC pairs are interfered, which is not required for, e.g., repeater protocols. We obtain a HOM visibility of $24.5 \pm 0.5\%$, as shown in Fig. 4(c). We subtract the multiphoton background determined through the detection of coincident counts when either of the two photon sources are blocked. The corrected interference pattern in Fig. 4(d) yields a HOM visibility of $97.1 \pm 1.7\%$,
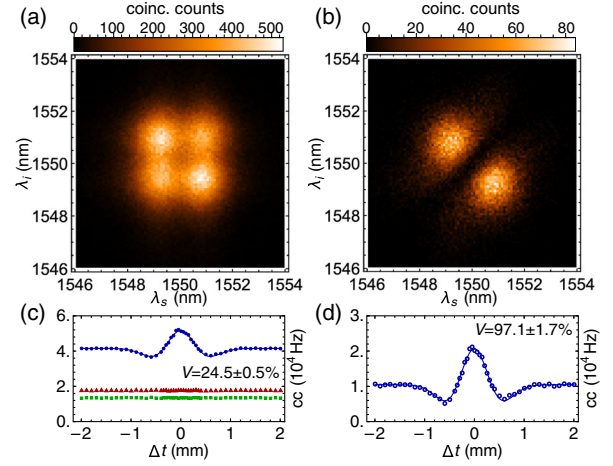

FIG. 4. Entanglement swapping results. (a) JSI reconstruction of the fully mixed state. The two peaks on the antidiagonal have higher count rates because the contribution from the $|\psi^-\rangle$ state is counted twice in the threefold coincidences. (b) JSI reconstruction of the entanglement-swapped state. We display a 8 nm spectral range with 0.118 nm bin size to highlight the main JSI features. (c) HOM data without signal error correction. The blue data points are the fourfold coincidence counts detected by the SNSPDs when both the sources are active, while red triangles and green squares are the error signals measured by alternately blocking one of the two sources. (d) HOM data, corrected for higher-order emissions.

certifying success of the TFM entanglement swapping protocol.

We can now reconstruct the effective JSA of the swapped state under the assumptions discussed earlier, calculating a Schmidt number of 2.15 ± 0.01—slightly higher than for the single-source scenario, as expected due to discrepancies between independent sources that affect the interference quality.

We have demonstrated the first instance of TFM entanglement generation enabled by nonlinearity engineering, achieving high generation rates, heralding efficiency and spectral entanglement. Due to its simplicity and quality, we expect this technique to be used in a host of different quantum information tasks. The flexibility in tailoring the PMF lends itself to the generation of high-dimensional TFM entanglement: not only can one use higher-order Hermite-Gaussian PMFs to upscale to qudits [10], but one can also aim at different PMF shapes for targeting specific applications, such as frequency multiplexing [35]. The same nonlinearity engineering technique can be used in asymmetric group-velocity matching condition [20] to generate pure, TFM-encoded single photons, as well as to implement mode filtering and TFM-projective measurements in a quantum pulse gate scheme, complementing the TFM framework based on pump spectral-shaping [5,10]. Finally, the ability to customize biphoton spectra could be useful for multiphoton quantum metrology applications in which measurement precision depends on the shape and steepness of the HOM pattern [36].

Note added.—Recently, a similar experiment has been reported [37] where TFM entanglement swapping is heralded by a frequency-resolved Bell-state measurement, and verified using a similar scheme.

———

[*]fraccalo@gmail.com
[†]These two authors contributed equally.

[1] M. Erhard, M. Malik, M. Krenn, and A. Zeilinger, Experimental Greenberger-Horne-Zeilinger entanglement beyond qubits, Nat. Photonics **12**, 759 (2018).

[2] J. Wang, S. Paesani, Y. Ding, R. Santagati, P. Skrzypczyk, A. Salavrakos, J. Tura, R. Augusiak, L. Mančinska, D. Bacco, D. Bonneau, J. W. Silverstone, Q. Gong, A. Acín, K. Rottwitt, L. K. Oxenløwe, J. L. O'Brien, A. Laing, and M. G. Thompson, Multidimensional quantum entanglement with large-scale integrated optics, Science **360**, 285 (2018).

[3] N. J. Cerf, M. Bourennane, A. Karlsson, and N. Gisin, Security of Quantum Key Distribution Using *d*-Level Systems, Phys. Rev. Lett. **88**, 127902 (2002).

[4] M. Huber and M. Pawłowski, Weak randomness in device-independent quantum key distribution and the advantage of using high-dimensional entanglement, Phys. Rev. A **88**, 032309 (2013).

[5] B. Brecht, D. V. Reddy, C. Silberhorn, and M. G. Raymer, Photon Temporal Modes: A Complete Framework for Quantum Information Science, Phys. Rev. X **5**, 041017 (2015).

[6] M. Kues, C. Reimer, P. Roztocki, L. R. Cortés, S. Sciara, B. Wetzel, Y. Zhang, A. Cino, S. T. Chu, B. E. Little, D. J. Moss, L. Caspani, J. Azaña, and R. Morandotti, On-chip generation of high-dimensional entangled quantum states and their coherent control, Nature (London) **546**, 622 (2017).

[7] N. T. Islam, C. C. W. Lim, C. Cahall, J. Kim, and D. J. Gauthier, Provably secure and high-rate quantum key distribution with time-bin qudits, Sci. Adv. **3**, e1701491 (2017).

[8] H.-H. Lu, J. M. Lukens, N. A. Peters, B. P. Williams, A. M. Weiner, and P. Lougovski, Quantum interference and correlation control of frequency-bin qubits, Optica **5**, 1455 (2018).

[9] P. Imany, J. A. Jaramillo-Villegas, M. S. Alshaykh, J. M. Lukens, O. D. Odele, A. J. Moore, D. E. Leaird, M. Qi, and A. M. Weiner, High-dimensional optical quantum logic in large operational spaces, npj Quantum Inf. **5**, 59 (2019).

[10] V. Ansari, J. M. Donohue, B. Brecht, and C. Silberhorn, Tailoring nonlinear processes for quantum optics with pulsed temporal-mode encodings, Optica **5**, 534 (2018).

[11] Q. Ding, R. Chatterjee, Y. Huang, and T. Yu, High-dimensional temporal mode propagation in a turbulent environment, arXiv:1907.02321.

[12] A. Eckstein, B. Brecht, and C. Silberhorn, A quantum pulse gate based on spectrally engineered sum frequency generation, Opt. Express **19**, 13770 (2011).

[13] A. Pe'er, B. Dayan, A. A. Friesem, and Y. Silberberg, Temporal Shaping of Entangled Photons, Phys. Rev. Lett. **94**, 073601 (2005).

[14] N. Matsuda, Deterministic reshaping of single-photon spectra using cross-phase modulation, Sci. Adv. **2**, e1501223 (2016).

[15] V. Averchenko, D. Sych, G. Schunk, U. Vogl, C. Marquardt, and G. Leuchs, Temporal shaping of single photons enabled by entanglement, Phys. Rev. A **96**, 043822 (2017).

[16] C. J. McKinstrie, J. B. Christensen, K. Rottwitt, and M. G. Raymer, Generation of two-temporal-mode photon states by vector four-wave mixing, Opt. Express **25**, 20877 (2017).

[17] S. Francesconi, F. Baboux, A. Raymond, N. Fabre, G. Boucher, A. Lemaître, P. Milman, M. Amanti, and S. Ducci, Engineering two-photon wavefunction and exchange statistics in a semiconductor chip, arXiv:1907.07935.

[18] F. Graffitti, D. Kundys, D. T. Reid, A. M. Brańczyk, and A. Fedrizzi, Pure down-conversion photons through sub-coherence-length domain engineering, Quantum Sci. Technol. **2**, 035001 (2017).

[19] F. Graffitti, P. Barrow, M. Proietti, D. Kundys, and A. Fedrizzi, Independent high-purity photons created in domain-engineered crystals, Optica **5**, 514 (2018).

[20] F. Graffitti, J. Kelly-Massicotte, A. Fedrizzi, and A. M. Brańczyk, Design considerations for high-purity heralded single-photon sources, Phys. Rev. A **98**, 053811 (2018).

[21] See Supplemental Material at http://link.aps.org/supplemental/10.1103/PhysRevLett.124.053603 for additional details regarding experimental methods and extended theoretical derivations.

[22] Y.-P. Huang and P. Kumar, Mode-resolved photon counting via cascaded quantum frequency conversion, Opt. Lett. **38**, 468 (2013).

[23] V. Ansari, J. M. Donohue, M. Allgaier, L. Sansoni, B. Brecht, J. Roslund, N. Treps, G. Harder, and C. Silberhorn, Tomography and Purification of the Temporal-Mode Structure of Quantum Light, Phys. Rev. Lett. **120**, 213601 (2018).

[24] D. V. Reddy and M. G. Raymer, High-selectivity quantum pulse gating of photonic temporal modes using all-optical Ramsey interferometry, Optica **5**, 423 (2018).

[25] I. Jizan, B. Bell, L. G. Helt, A. C. Bedoya, C. Xiong, and B. J. Eggleton, Phase-sensitive tomography of the joint spectral amplitude of photon pair sources, Opt. Lett. **41**, 4803 (2016).

[26] A. O. C. Davis, V. Thiel, and B. J. Smith, Measuring the quantum state of a photon pair entangled in frequency and time, arXiv:1809.03727.

[27] I. Gianani, Robust spectral phase reconstruction of time-frequency entangled bi-photon states, Phys. Rev. Research **1**, 033165 (2019).

[28] M. Avenhaus, A. Eckstein, P. J. Mosley, and C. Silberhorn, Fiber-assisted single-photon spectrograph, Opt. Lett. **34**, 2873 (2009).

[29] C. K. Hong, Z. Y. Ou, and L. Mandel, Measurement of Subpicosecond Time Intervals between Two Photons by Interference, Phys. Rev. Lett. **59,** 2044 (1987).

[30] R.-B. Jin, T. Gerrits, M. Fujiwara, R. Wakabayashi, T. Yamashita, S. Miki, H. Terai, R. Shimizu, M. Takeoka, and M. Sasaki, Spectrally resolved Hong-Ou-Mandel interference between independent photon sources, Opt. Express **23,** 28836 (2015).

[31] A. Fedrizzi, T. Herbst, M. Aspelmeyer, M. Barbieri, T. Jennewein, and A. Zeilinger, Anti-symmetrization reveals hidden entanglement, New J. Phys. **11,** 103052 (2009).

[32] T. Douce, A. Eckstein, S. P. Walborn, A. Z. Khoury, S. Ducci, A. Keller, T. Coudreau, and P. Milman, Direct measurement of the biphoton Wigner function through two-photon interference, Sci. Rep. **3,** 3530 (2013).

[33] A. M. Brańczyk, Hong-Ou-Mandel interference, arXiv:1711 .00080.

[34] D. L. P. Vitullo, M. G. Raymer, B. J. Smith, M. Karpiński, L. Mejling, and K. Rottwitt, Entanglement swapping for generation of heralded time-frequency-entangled photon pairs, Phys. Rev. A **98,** 023836 (2018).

[35] T. Hiemstra, T. F. Parker, P. C. Humphreys, J. Tiedau, M. Beck, M. Karpiński, B. J. Smith, A. Eckstein, W. S. Kolthammer, and I. A. Walmsley, Pure single photons from scalable frequency multiplexing, arXiv:1907.10355.

[36] A. Lyons, G. C. Knee, E. Bolduc, T. Roger, J. Leach, E. M. Gauger, and D. Faccio, Attosecond-resolution Hong-Ou-Mandel interferometry, Sci. Adv. **4,** eaap9416 (2018).

[37] S. Merkouche, V. Thiel, A. O. C. Davis, and B. J. Smith, Two-color Bell states heralded via entanglement swapping, arXiv:1910.06506.